Inhibitor	$MycP_{1mth}$ inhibition (%)
Halt™ protease inhibitor cocktail (2X) (2 mM AEBSF, 1.6 uM Aprotinin, 100 μM Bestatin, 30 μM E64, 40 μM Leupeptin, 20 μM Pepstatin, 10 mM EDTA)	33.8%
MeOSuc-Ala-Ala-Pro-Val-CMK (Elastase inhibitor III) (150 μM)	3.4%
MeOSuc-Ala-Ala-Pro-Ala-CMK (Elastase inhibitor II) (150 μM)	3.3%
Aminoethyl-benzene sulfonyl fluoride Hydrochloride (AEBSF) (100 μM)	none detected
Phenylmethanesulfonyl Fluoride (PMSF) (100 μM)	none detected

Supplementary Table 1.

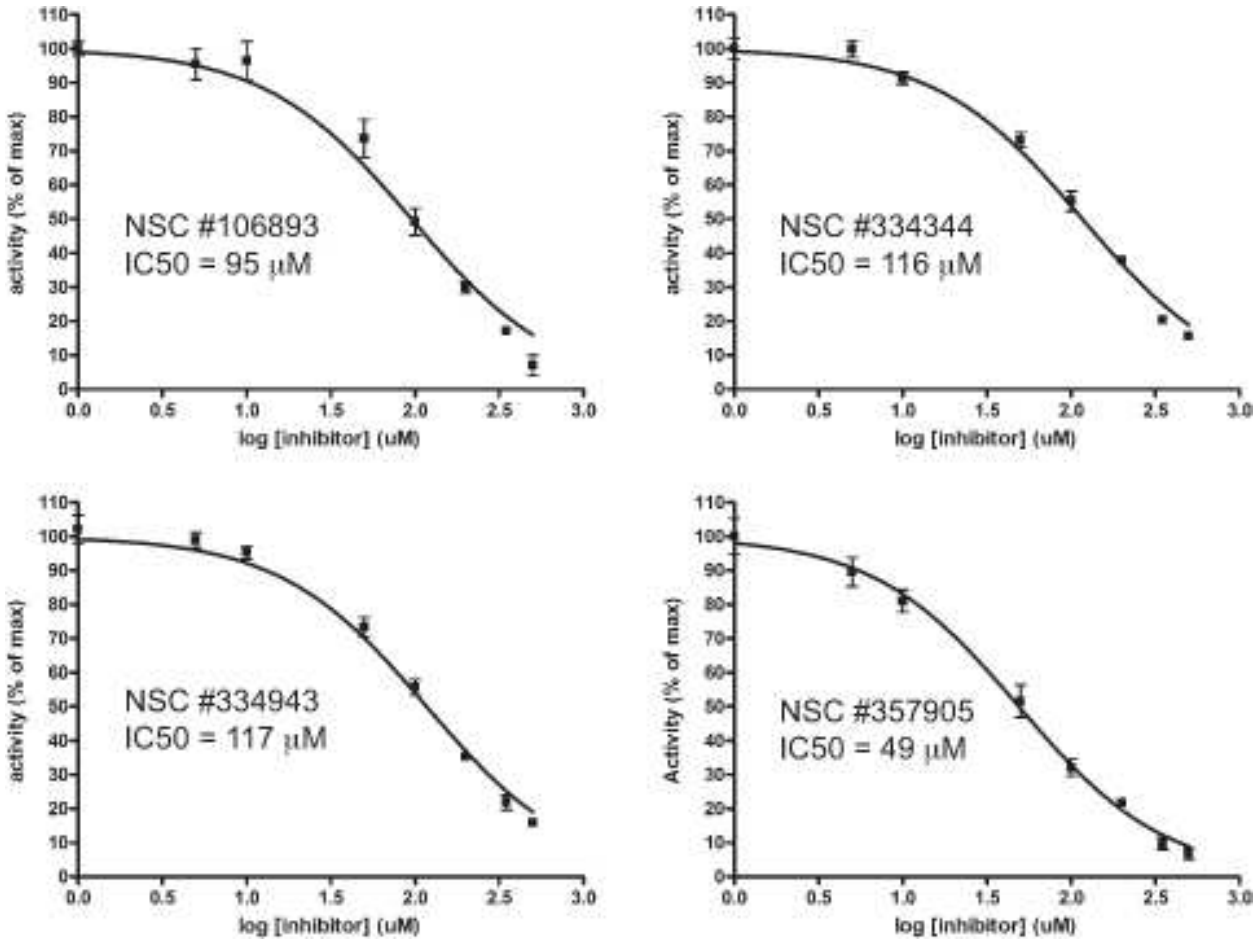

Supplementary Figure 1. Dose response curves of $MycP_1$ inhibitors. The compounds were added at varying concentrations and the dose response was graphed using the sigmoidal dose-response function in Graphpad Prism. The curve was constrained to approach 100% activity at the top and no activity at the bottom of the curve. Error bars represent the standard error at each concentration for three experiments.

Molecular modeling of the binding peptide with $MycP_1$. The multiple conformational states of the peptide were generated using OMEGA (Open Eye Scientific Software). The docking poses of the peptide multi-conformation structures (ligands) were performed using SABRE$^{Lig\text{-}Rec}$ software. The docking strategy exhaustively docked/scored all possible positions of each ligand (each peptide conformation) in the $MycP_1$ (PDBID 4HVL)[1] binding site. The rigid docking roughly consisted of two steps - shape fitting and application of optimization filters. During the shape fitting, the ligand (peptide structure) was placed into a 0.5 Å resolution grid box encompassing all active-site atoms (including hydrogen atoms) using smooth Gaussian potential. Two optimization filters were subsequently processed - rigid-body optimization and optimization of the ligand pose in the dihedral angle space. The pose ensemble was filtered to reject poses that did not have sufficient shape complementarity with the active site of the protein followed by rejection of those lacking at least one heavy atom hydrogen bond with the carbonyl group of Ser202 backbone. In separate docking runs, the binding poses of the ligand structure were refined by MD simulations followed by MM-GBSA calculations using Sander module from Amber11 package[2] as previously described.[3]

Briefly, the $MycP_1$-peptide binding complex was neutralized by adding appropriate counter ions and was solvated in a rectangular box of TIP3P water molecules with a minimum solute-wall distance of 10 Å. The solvated systems were energy-minimized and carefully equilibrated. These systems were gradually heated from T = 10 K to T = 298.15 K in 50 ps before running an MD simulation. The MD simulations were performed with a periodic boundary condition in the NPT ensemble at T = 298.15 K with Berendsen temperature coupling[4] and constant pressure (P=1 atm) with isotropic molecule-based scaling. A time step of 2.0 fs was used, with a cutoff of 12 Å for the nonbonded interactions, and the SHAKE algorithm was employed to keep all bonds involving hydrogen atoms rigid.[5] Long-range interactions were handled using the particle mesh Ewald (PME) algorithm.[6] During the energy minimization and MD simulation, only the ligand (peptide) and residue side chains in the binding pocket were permitted to move. We used this constraint to prevent any changes in the $MycP_1$ structure due to the presence of residues in the loops on the top of the protein active site. A residue-based cutoff of 12 Å was utilized for non-covalent interactions. MD simulations were then carried out for ~8.0 ns. During the simulations,

---

1 Wagner JM, Evans TJ, Chen J, Zhu H, Houben EN, Bitter W, Korotkov KV. Understanding specificity of the mycosin proteases in ESX/type VII secretion by structural and functional analysis. *J Struct Biol*. **2013**; *184* (2), 115-28.

(2)Case, D. A.; Darden, T. A.; Cheatham, T. E.; Simmerling, C. L.; Wang, J.; Duke, R. E.; Luo, R.; Crowley, M.; Walker, R. C.; Zhang, W.; Merz, K. M.; Wang, B.; Hayik, S.; Roitberg, A.; Seabra, G.; Kolossváry, I.; Wong, K. F.; Paesani, F.; Vanicek, J.; Wu, X.; Brozell, S. R.; Steinbrecher, T.; Gohlke, H.; Yang, L.; Tan, C.; Mongan, J.; Hornak, V.; Cui, G.; Mathews, D. H.; Seetin, M. G.; Sagui, C.; Babin, V.; Kollman, P. A., AMBER 10. *San Francisco, CA: University of California* **2008.**

(3)(a) Hamza, A.; Zhao, X.; Tong, M.; Tai, H. H.; Zhan, C. G.*Bioorg. Med. Chem.* **2011,***19*, 6077-6086;(b) Bargagna-Mohan, P.; Paranthan, R. R.; Hamza, A.; Dimova, N.; Trucchi, B.; Srinivasan, C.; Elliott, G. I.; Zhan, C. G.; Lau, D. L.; Zhu, H. Y.; Kasahara, K.; Inagaki, M.; Cambi, F.; Mohan, R.*J. Biol. Chem.* **2010,***285*, 7657-7669.

(4) Berendsen, H. J. C.; Postma, J. P. M.; Vangunsteren, W. F.; Dinola, A.; Haak, J. R., Molecular-dynamics with coupling to an external bath. *J. Chem. Phys.* **1984,** *81* (8), 3684-3690.

(5) Ryckaert, J. P.; Ciccotti, G.; Berendsen, H. J. C., Numerical-integration of cartesian equations of motion of a system with constraints - molecular-dynamics of n-alkanes. *J. Comput. Phys.* **1977,** *23* (3), 327-341.

(6) Darden, T.; York, D.; Pedersen, l., Particle Mesh Ewald - Nn n.log(n) method for ewald sums in large systems. *J. Chem. Phys.* **1993,** *98* (12), 10089-10092.

the coordinates of the system were collected every 1 ps. The last 100 snapshots of the simulated structure of the MD trajectory were used to perform the MM-GBSA calculations.

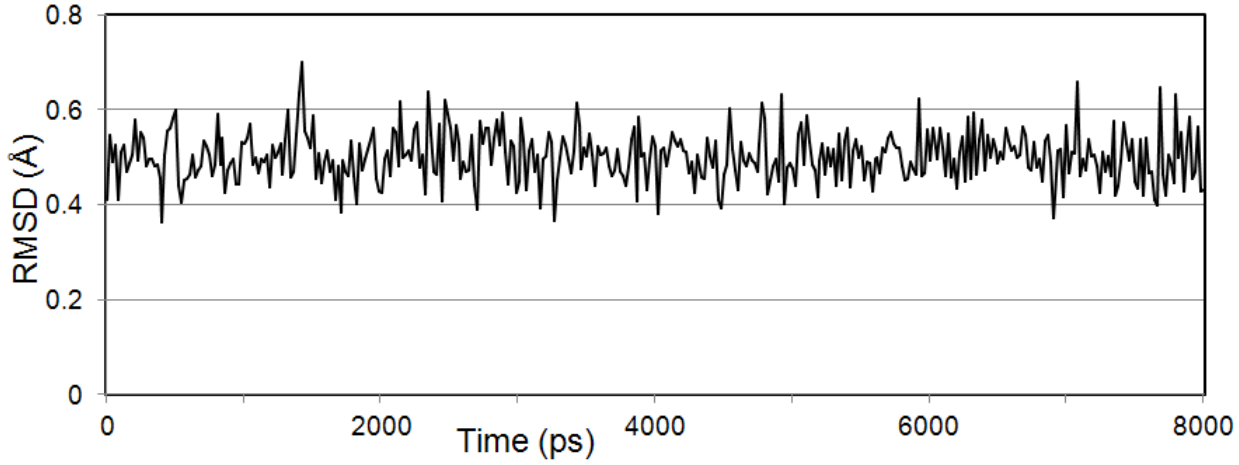

Supplementary Figure 2. MD simulated RMSD of the Cα peptide backbone.

structure	1	2	3	4	5	6	7	8	9	10
1	1.000	0.459	0.776	0.484	0.525	0.444	0.382	0.276	0.313	0.339
2	0.459	1.000	0.485	0.395	0.425	0.413	0.400	0.308	0.321	0.284
3	0.776	0.485	1.000	0.425	0.522	0.359	0.321	0.239	0.241	0.313
4	0.484	0.395	0.425	1.000	0.467	0.508	0.423	0.358	0.379	0.394
5	0.525	0.425	0.522	0.467	1.000	0.409	0.380	0.328	0.258	0.200
6	0.444	0.413	0.359	0.508	0.409	1.000	0.516	0.682	0.615	0.293
7	0.382	0.400	0.321	0.423	0.380	0.516	1.000	0.364	0.411	0.300
8	0.276	0.308	0.239	0.358	0.328	0.682	0.364	1.000	0.595	0.224
9	0.313	0.321	0.241	0.379	0.258	0.615	0.411	0.595	1.000	0.277
10	0.339	0.284	0.313	0.394	0.200	0.293	0.300	0.224	0.277	1.000

Supplementary Table 2. Pair-wise similarity of the 10 lead compounds using MACCS fingerprints.

Compound ID	Name
NSC-334943	N-(2-((2-amino-1-benzyl-2-oxoethyl)amino)-1-methyl-2-oxoethyl)-3-(2-furyl)acrylamide
UC-521228	2-Bromo-N-{(2S)-1-[(4-nitrophenyl)amino]-2-propanyl}benzamide
NSC-334344	N-(2-((1-(aminocarbonyl)-3-methylbutyl)amino)-2-oxoethyl)-3-(2-furyl)acrylamide
NSC-657705	N-(2-methylphenyl)-2-(2-(2-(2-oxo-1,2-dihydro-3H-indol-3-ylidene)hydrazino)-1,3-thiazol-4-yl)acetamide
NSC-112182	methyl 4-(methylthio)-2-((2-((2-quinoxalinylcarbonyl)amino)propanoyl)amino)butanoate
NSC-25812	2-cyano-2-((2-methoxyphenyl)diazenyl)acetamide
NSC-176297	4-(2-(2-amino-1-cyano-2-oxoethylidene)hydrazino)benzenesulfonic acid
NSC-106893	2-((3,4,5-trimethoxyphenyl)hydrazono)malononitrile
NSC-97914	3-oxo-3-phenyl-2-(phenylhydrazono)propanenitrile
NSC-357905	N",N""-2,5(1H,4H)-Pentalenediylidenedicarbonohydrazonic diamide

Supplementary Table 3. Names of the lead compounds.

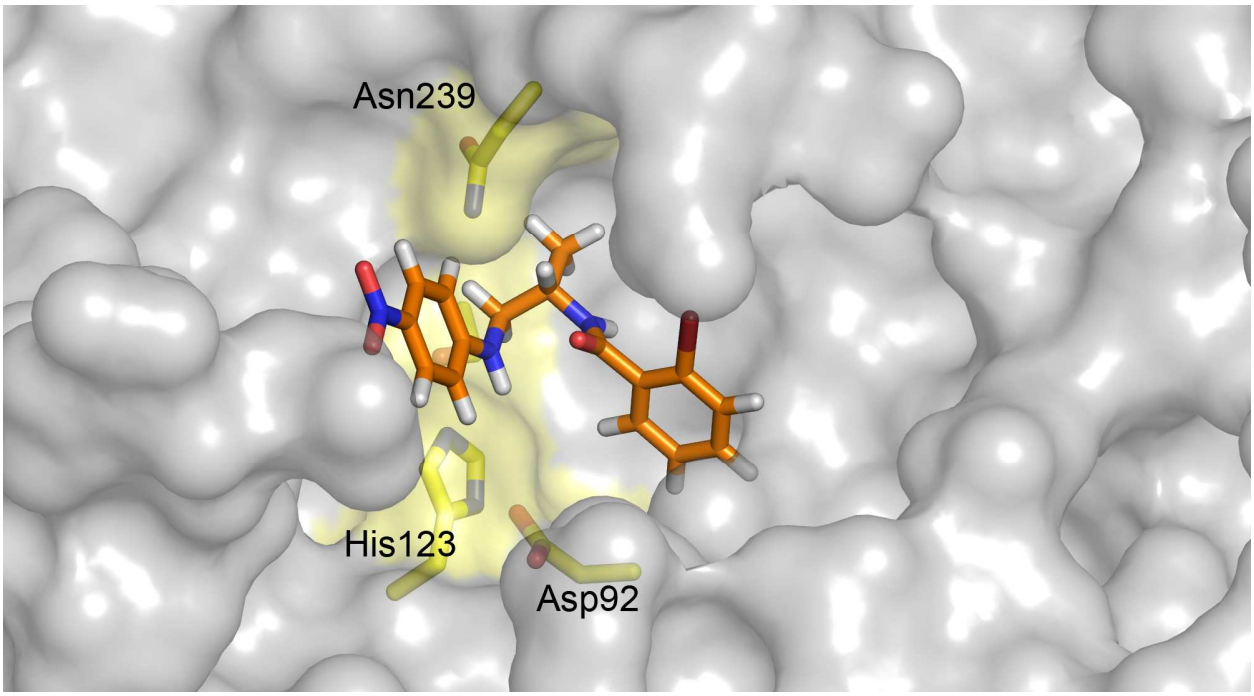

Supplementary Figure 3. Surface view of the $MycP_1$ active site with compound **2** docked. The key catalytic site residues are highlighted.

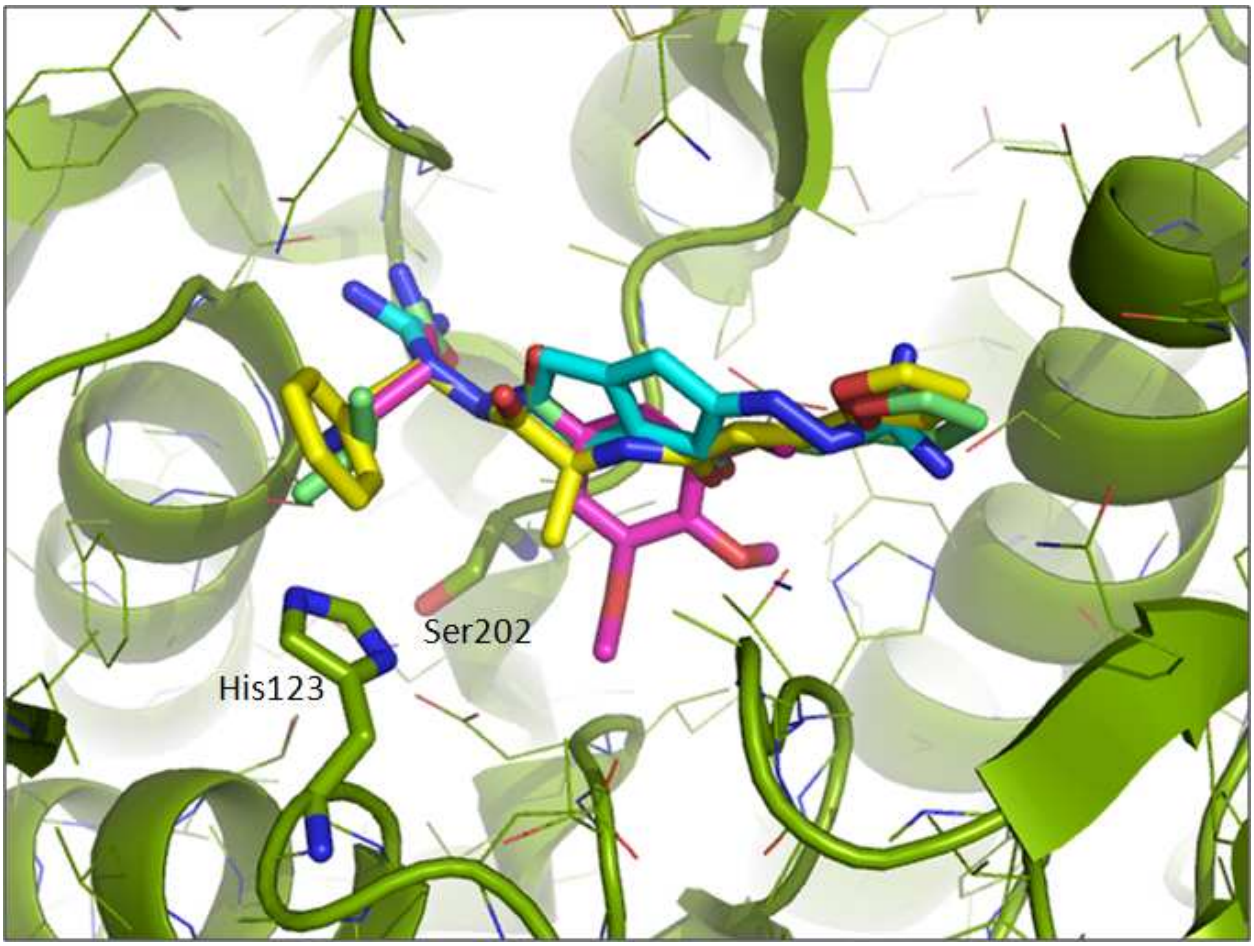

Supplementary Figure 4. Ribbon view of the $MycP_1$ active site (pdb: 4HVL) with the binding lead compounds (**1**, **3**, **8**, and **10**)